# On Modeling and Control of the Retraction Phase for Airborne Wind Energy Systems

Aldo U. Zgraggen*, Lorenzo Fagiano, and Manfred Morari

***Abstract*— The retraction phase of a ground-based airborne wind energy system is the second part of a two phase power generation cycle. In the first phase, energy is produced by exploiting the aerodynamic lift exerted by a wing tethered to the ground and controlled to fly crosswind paths. Power is produced by unreeling the tether, wound around drums connected to generators, under high traction force. In the retraction phase, the tether is reeled-in after its maximum length has been reached. In this paper, a new control-oriented model for the retraction phase is derived from first principles, and a flight controller based on this model, which is straightforward to implement and tune, is proposed. Simulation results comparing this new strategy to an existing approach are presented. The main advantage of the new approach is that it uses readily available measurements for feedback control, hence resulting in a more robust and reliable solution.**

## I. Introduction

Airborne wind energy (AWE) systems aim to overcome the height limit of traditional wind mills imposed by their large rigid structure. By employing wings tethered to the ground, AWE systems are able to harness wind energy beyond the altitude of traditional wind mills, in stronger and more steady winds, see [1], [2] for an overview.

The wing's motion is influenced by the so called steering input, which typically corresponds to a change of the roll angle of the wing, and can be actuated by means of different possible technical solutions, e.g. changing the relative length of the steering lines. The path of the wing is restricted on a spherical surface with a radius equals the tether length, confined by the ground and by a vertical plane perpendicular to the wind direction. This spherical surface is commonly called "wind window".

Depending on the flown path of the wing in the wind window, a higher or lower traction force is experienced. For paths at low elevations and roughly aligned with the wind direction, i.e. so called crosswind paths where the wind flow is roughly aligned with the tether, a high wing speed results and thus a high traction is exerted. On the other hand, if the wing is flown on the side of the wind window, i.e a position roughly perpendicular to the wind direction at the border of the wind window against the wind, a low wing speed will results and a small traction force is exerted.

A. Zgraggen, and M. Morari are with Automatic Control Laboratory, Swiss Federal Institute of Technology, Switzerland. zgraggen|morari@control.ee.ethz.ch

L. Fagiano is with Corporate Research Center, ABB Schweiz Ltd., Switzerland. lorenzo.fagiano@ch.abb.ch

This research has received partial funding from the Swiss Competence Center Energy and Mobility (CCEM). The authors acknowledge the SpeedGoat® 's Greengoat program.

* Corresponding author: zgraggen@control.ee.ethz.ch.

In this paper, ground-based generation is considered where a two-phase cycle, or power cycle, is carried out exploiting the traction force on the tether, see e.g. [3], [4]. In the first phase of the two-phase cycle, the traction phase, energy is produced by unreeling the tether from the drums under large traction force by flying a crosswind path. Once the tether has reached its maximum length, the second phase, the retraction phase, starts by recoiling the cable under minimal load by flying the wing on the side of the wind window and consuming only a fraction of the energy previously produced.

The automatic control of tethered wings plays a major role for the operation of this kind of system and has been studied in various publications, see [4], [5], [6], [7], [8], [9], [10], [11]. Most of these approaches consider only the problem of flying crosswind figures where the energy is produced. However, for ground-based generation systems also the retraction of the tether has to be done autonomously. In [4] and [5] a controller for the retraction phase, using a nonlinear Model Predictive Control strategy, has been proposed. However, these control strategies might be difficult to implement and tune, due to their complexity. Additionally, they assume a quite good knowledge of the wind speed at the wing's location which might be hard to obtain in practice.

In [12], a linear control approach based on the notion of the velocity angle, describing the wing's flying direction, has been introduced to retract the wing at the side of the wind window keeping it at a static angular position relative to the ground unit (GU) such that the exerted traction force is minimal. In this paper, we study the dynamics of such a maneuver and propose a model relating the steering input directly to the elevation of the wing. This model is then used to design a hierarchical control system which is simple to tune and able to stabilize the wing's trajectory at a constant elevation angle during the retraction phase. Additionally, the proposed approach is independent of an estimate of the velocity angle and only relies on directly measurable variables, hence resulting in a more reliable and robust solution with respect to the one presented in [12]. We support this consideration by presenting simulation results where the two approaches are compared, using a nonlinear model of the system.

## II. System Description

The system under consideration is related to the Swiss Kite Power prototype [13], see Fig. 1. It is a AWE system featuring ground-based steering actuators with the generators placed in the GU. It has three drums with a motor connected to each of it, and it can be used with one, two and three-line

wings or power kites. During the traction phase the motors act as generators by unreeling the lines under load and during the retraction phase they are used to recoil the tethers. For three-line systems, the line wound around the middle drum, called power line, is connected to the leading edge of the wing and sustains the main portion of the traction force. The lines on the other two drums are called steering lines and are connected to the left and right wing tips. By changing the relative line length $\delta$ of the two steering lines the wing can be steered. A shorter left line induces a counter-clockwise turn of the wing as seen from the GU, and vice-versa. The system has a total rated power of 20 kW; the generator of the middle drum has a power rating of 10 kW and each of the motors connected to the drums of the steering lines have a power rating of 5 kW. The system is operated with tether lengths up to 200 m. Next, we recall a dynamical model of the described system and the definition of the velocity angle $\gamma$, which acts as one of the main feedback variables during the traction phase [14].

Fig. 1: Lead-out sheaves of the Swiss Kite Power prototype while flying a three line kite.

### A. Model Equations

The dynamical model we consider has been widely used in previous works, see e.g. [4] and references therein. We will recall the model equations shortly, following the same notation as in [14]. We will denote vector valued variable in bold, e.g. ${}_G\mathbf{p}(t)$, where the subscript letter in front of vectors denote the reference system considered to express the vector components and $t$ denotes the time dependence.

An inertial frame centered at the GU is denoted as $G \doteq (\mathbf{e}_x, \mathbf{e}_y, \mathbf{e}_z)$, where unit vectors are denoted by $\mathbf{e}$ with the corresponding direction indicated by the trailing subscript letter. The $\mathbf{e}_x$ axis is assumed to be parallel to the ground, contained in the longitudinal symmetry plane of the GU, the $\mathbf{e}_z$ axis is pointing upwards, and the $\mathbf{e}_y$ axis is such that it forms a right hand system. The wing's position vector ${}_G\mathbf{p}(t)$ can be expressed in the inertial frame using spherical coordinates $(\varphi(t), \vartheta(t), r(t)))$ as (see Fig. 2):

$$ {}_G\mathbf{p}(t) = \begin{pmatrix} r(t)\cos(\varphi(t))\cos(\vartheta(t)) \\ r(t)\sin(\varphi(t))\cos(\vartheta(t)) \\ r(t)\sin(\vartheta(t)) \end{pmatrix}. \tag{1} $$

Note that all three variables $(\varphi(t), \vartheta(t), r(t)))$ can be measured directly with good accuracy by devices installed on the ground such as line angle sensors and motor encoders.

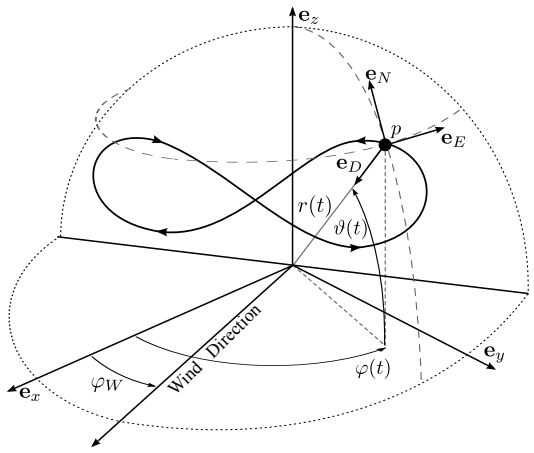


Fig. 2: The wing's position $p$ (black dot) is shown on a figure eight path together with the local coordinate frame $L$.

The motion of the tethered wing is restricted on a spherical surface with radius $r(t)$ confined by the ground plane $(\mathbf{e}_x, \mathbf{e}_y)$ and a vertical plane perpendicular to the wind direction $\varphi_W$. This spherical surface is called "wind window" (see Fig. 2, dotted lines). If $r(t)$ is kept constant, the vertical plane contains the anchor point and the wind window corresponds to a quarter sphere. Otherwise, depending on the reeling speed $\dot{r}(t)$ of the tether, the wind window contains a larger or smaller surface area than a quarter sphere. For example with $\dot{r}(t) < 0$, i.e. reeling-in the tether, the wing is able to surpass the GU against the wind direction.

We also define a non-inertial coordinate system $L \doteq (\mathbf{e}_N, \mathbf{e}_E, \mathbf{e}_D)$, centered at the wing's position (depicted in Fig. 2). The $\mathbf{e}_N$ axis, or local north, is tangent to the sphere of radius $r(t)$, on which the wing's trajectory evolves, and points towards its zenith. The $\mathbf{e}_D$ axis, called local down, points to the center of the sphere (i.e the GU), hence is perpendicular to the tangent plane of the sphere at the wing's position. The $\mathbf{e}_E$ axis, named local east, forms a right hand system and spans the tangent plane together with $\mathbf{e}_N$. The system $L$ is a function of the wing's position only. The transformation matrix to express the vectors in the local frame $L$ from the inertial frame $G$ is denoted by $A_{LG}$ (e.g. ${}_L\mathbf{p}(t) = A_{LG}\,{}_G\mathbf{p}(t)$):

$$ A_{LG} = \begin{pmatrix} -\sin(\vartheta)\cos(\varphi) & -\sin(\vartheta)\sin(\varphi) & \cos(\vartheta) \\ -\sin(\varphi) & \cos(\varphi) & 0 \\ -\cos(\vartheta)\cos(\varphi) & -\cos(\vartheta)\sin(\varphi) & -\sin(\vartheta) \end{pmatrix}. \tag{2} $$

From the differentiation of (1) and using the rotation matrix (2) we obtain the velocity vector of the wing in local

coordinates $L$ with respect to the GU as:

$$ {}_L\mathbf{v}_P(t) = \begin{pmatrix} r(t)\dot{\vartheta}(t) \\ r\cos\vartheta(t)\,\dot{\varphi}(t) \\ \dot{r}(t) \end{pmatrix}. \tag{3} $$

The dynamic equations of the model are derived from first principles and the wing is assumed to be a point with given mass. The tether is assumed to be straight with a non-zero diameter. The aerodynamic drag of the tether and the tether mass are added to the wing's drag and mass, respectively. The effects of gravity and inertial forces are also considered. The wing is assumed to be steered by a change of the roll angle $\psi(t)$, which is manipulated by the control system via the line length difference. By applying Newton's law of motion to the wing in the reference system $L$ we obtain:

$$ \left| \begin{array}{rcl} \ddot{\vartheta} & = & \frac{\mathbf{F}\cdot\mathbf{e}_N}{rm} - \sin(\vartheta)\cos(\vartheta)\dot{\varphi}^2 - \frac{2}{r}\dot{\vartheta}\dot{r} \\ \ddot{\varphi} & = & \frac{\mathbf{F}\cdot\mathbf{e}_E}{rm\cos(\vartheta)} + 2\tan(\vartheta)\dot{\vartheta}\dot{\varphi} - \frac{2}{r}\dot{\varphi}\dot{r} \\ \ddot{r} & = & -\frac{\mathbf{F}\cdot\mathbf{e}_D}{m} + r\dot{\vartheta}^2 + r\cos^2(\vartheta)\dot{\varphi}^2 \end{array} \right|, \tag{4} $$

where $m$ is the mass of the wing. The force $\mathbf{F}(t)$ consist of contributions from gravity and aerodynamic forces, see [14] for details. Note that for simplicity of notation we dropped the time dependence of the involved variables in (2) and (4).

In a recent contribution concerned with the autonomous flight along figure eight paths during traction phase, the notion of the velocity angle $\gamma$ has been introduced (see [14]), defined as:

$$ \gamma(t) \doteq \arctan\left(\frac{\mathbf{v}_P(t)\cdot\mathbf{e}_E(t)}{\mathbf{v}_P(t)\cdot\mathbf{e}_N(t)}\right) \tag{5} $$

$$ = \arctan\left(\frac{\cos\vartheta(t)\,\dot{\varphi}(t)}{\dot{\vartheta}(t)}\right). \tag{6} $$

Thus, the angle $\gamma(t)$ is the angle between the local north $\mathbf{e}_N(t)$ and the projection of the wing's velocity vector $\mathbf{v}_P(t)$ onto the tangent plane of the wind window. In (6) the four-quadrant version of the arc tangent function shall be used, such that $\gamma(t) \in [-\pi, \pi]$.

The velocity angle is particularly suited as a feedback variable for the traction phase since it describes the flight conditions of the wing with just one scalar: as an example, if $\gamma = 0$ the wing is moving upwards towards the zenith of the wind window, if $\gamma = \pi/2$ the wing is moving parallel to the ground towards the local east, finally if $\gamma = \pi$ the wing is flying towards the ground. Additionally, a control-oriented model for tethered wings, originally proposed by [15] and refined in [14], has been used for the control design of the traction phase:

$$ \dot{\gamma}(t) \simeq K(t)\delta(t) + T(t), \tag{7} $$

where

$$ K(t) = \frac{\rho C_L(t) A |\mathbf{v}(t)|}{2 m d_s}\left(1 + \frac{1}{E_{eq}^2(t)}\right)^2 \tag{8a} $$

$$ T(t) = \frac{g\cos\vartheta(t)\,\sin\gamma(t)}{|\mathbf{v}(t)|} + \sin\vartheta(t)\,\dot{\varphi}(t). \tag{8b} $$

In (7) and (8) the steering input, i.e. the line length difference of the steering lines, is denoted by $\delta(t)$, $\rho$ is the air density, $C_L(t)$ is the aerodynamic lift coefficient, $A$ is the reference area of the wing, $d_s$ is the span of the wing, $E_{eq}$ is the equivalent efficiency of the wing $E_{eq} \doteq C_L(t)/C_{D,eq}(t)$ where $C_{D,eq}(t)$ represents the drag coefficient of the wing and lines together, and $g$ is the gravity acceleration. In (8), the apparent wind speed is denoted by $\mathbf{v}(t)$, defined as

$$ \mathbf{v}(t) = \mathbf{v}_W(t) - \mathbf{v}_P(t), \tag{9} $$

where $\mathbf{v}_W(t)$ is the wind velocity vector assumed to be horizontal and at an angle $\varphi_W$ relative to $\mathbf{e}_x$, see Fig. 2.

The model (7) has been validated through experimental data with good correspondence in a wide range of operating conditions, see [14]. It was derived assuming crosswind flight conditions as performed during the traction phase.

During retraction, the tethers have to be recoiled onto the drums under minimal force, such that only a small fraction of the previously generated power is used. To achieve this goal with no pitch control, the wing has to be flown at the border of the wind window, in a static angular position w.r.t. GU, i.e. with constant or slowly varying $\varphi$ and $\vartheta$ angles. This represents quite a different flight condition with respect to the one assumed in (7). However, it has been shown that the model (7) can also, with some modifications, be used to describe the wing's steering dynamics during the retraction phase [12], employing a slightly changed definition of the velocity angle (6) called "regularized velocity angle".

An alternative approach to design a retraction controller, which is presented in this paper, is to exploit the coupling of the $\vartheta$-dynamics of a tethered wing during retraction with the steering input $\delta$. We will next recall shortly the results from [12] followed by an analysis of the $\vartheta$-dynamics during the retraction phase. The latter is then exploited in the proposed controller for the retraction phase.

### *B. Regularized Velocity Angle*

The main difference between the traction and retraction phases is the magnitude of the wing's speed on the tangent plane to the wind window, denoted by $\mathbf{v}_P^p(t)$. During the retraction phase $\mathbf{v}_P(t)$ is low and mainly consists of the reel-in speed $\dot{r}$. Thus $\mathbf{v}_P^p(t)$ is close to zero and the apparent wind speed is determined only by the wind speed $\mathbf{v}_W$ and the reel-in speed $\dot{r}$. In these conditions, the velocity angle $\gamma$ as computed in (6) becomes undefined, so that this variable can not be used for feedback control anymore. Therefore, in [12] a regularized version of the velocity angle (6) has been defined such that it can still be used as feedback variable for the retraction phase of a ground-based generation AWE system, when $\mathbf{v}_P^p(t)$ is close to zero.

For the sake of completeness, such regularized velocity angle will be now recalled. Consider the wing in a static position in terms of $\varphi$ and $\vartheta$ w.r.t GU. In these conditions, the apparent velocity of the wing in the tangent plane to the wind window is equal to the wind velocity projected on the same plane. Since the wing is assumed to be aligned with

the wind direction, its orientation $\beta(t)$ w.r.t to the local north $\mathbf{e}_N$ can be defined, similarly to (5)-(6), as

$$\beta(t) \doteq \arctan\left(\frac{-_L\mathbf{v}_W(t)\cdot\mathbf{e}_E(t)}{-_L\mathbf{v}_W(t)\cdot\mathbf{e}_N(t)}\right) \tag{10}$$

$$= \arctan\left(\frac{\sin(\varphi-\varphi_W)}{\sin\vartheta\cos(\varphi-\varphi_W)}\right), \tag{11}$$

which is the angle between the local north $\mathbf{e}_N$ and the longitudinal symmetry axis of the wing. From (11), assuming without loss of generality $\varphi_W = 0$, one can see that $\beta$ converges to $\pm\pi/2$ if the wing approaches the border of the wind window, e.g $\varphi \approx \pm\pi/2$. An estimate of the wind direction $\varphi_W$, needed to compute the angle $\beta$, can be either obtained by measurements provided by ground based sensors or by processing the measurements of the line force collected during the traction phase, see e.g. [16].

The considerations presented so far lead to the idea of extending the definition of the velocity angle $\gamma$ by a regularization term such that the wing's orientation is also defined for static positions of the wing. In particular, the regularized velocity angle is defined as (compare with (11)):

$$\gamma^r = \arctan\left(\frac{\cos(\vartheta)\dot{\varphi} + c\sin(\varphi-\varphi_W)}{\dot{\vartheta} + c\sin\vartheta\cos(\varphi-\varphi_W)}\right), \tag{12}$$

where $c > 0$ is a scalar chosen by the control designer. In principle, the value of $c$ should reflect the magnitude of the absolute wind speed, which might be quite difficult to obtain. However, in simulations and experiments the system behavior resulted to be not sensitive to this quantity.

Thus, according to (12), during the traction phase when the speed of the wing is significantly larger than the wind speed we have $\gamma^r \approx \gamma$, but during the retraction phase, when the wing speed approaches zero, $\gamma^r$ still provides a reasonable value whereas $\gamma$ of (6) becomes undefined.

Using the regularized velocity angle $\gamma^r$ instead of $\gamma$ in (7) allows to design a similar control strategy for the retraction phase [12] as used in [14] during the traction phase. Such a control approach is recalled in section III-A.

### C. Wing Elevation Dynamics During Retraction

As an alternative to estimating the heading of the wing for controlling its trajectory during the retraction phase, we propose here to use the elevation angle $\vartheta$ as feedback variable. The main advantage of such an approach is a higher reliability, since the elevation is directly measured and there is no need to estimate the wind direction. We will carry out the controller's design on the basis of a new model that links the elevation dynamics to the steering input, which we derive next.

From (4), we can write the $\vartheta$ dynamics as:

$$\ddot{\vartheta} = \frac{\mathbf{F}\cdot\mathbf{e}_N}{rm} - \frac{2}{r}\dot{\vartheta}\dot{r} - \sin(\vartheta)\cos(\vartheta)\dot{\varphi}^2\,. \tag{13}$$

We consider the following assumptions:

*Assumption 1:* (Dominant aerodynamic forces) The elevation dynamics are dominated by the aerodynamic force components and effects from gravity and apparent forces are small. ■

*Assumption 2:* (Constant azimuthal position) The azimuthal position $\varphi$ of the wing during the retraction phase is constant. ■

*Assumption 3:* (Small roll angle) The control input $\psi$ is sufficiently small such that its trigonometric functions can be linearized. ■

Assumption 1 implies that at all times we have a sufficiently strong apparent wind speed to sustain the wing and keep the tether tensioned. In the case of weak wind, this can always be enforced by increasing the user-defined reel-in speed of the tether. Moreover, this also implies that the wing's longitudinal axis is aligned with the apparent wind direction. Assumption 2 implies that the sum of the forces acting on the wing in $\mathbf{e}_E$ direction is zero. Assumption 3 is also reasonable, since for example during our test flights the input stayed within $\psi \simeq \pm 18^\circ$. We can now state our theoretical result:

*Proposition 1:* Let assumptions 1-3 hold. Then, the $\vartheta$ dynamics (13) can be written as

$$\ddot{\vartheta} = -\mathcal{C}\delta - \frac{g\cos(\vartheta) + 2\dot{\vartheta}\dot{r}}{r}\,, \tag{14}$$

where

$$\mathcal{C} = \frac{\rho A C_L}{2rmd_s}\left(1 + \frac{1}{E_{eq}^2}\right) W_0 \sin(\varphi)|\mathbf{v}|\,, \tag{15}$$

with $W_0$ being the nominal wind speed.

*Proof:* See the Appendix. ■

The model in (14) gives a direct relationship between the input $\delta$ and the elevation of the wing $\vartheta$. It can therefore be used as a model for the controller synthesis.

## III. Retraction Control Scheme

In this section we will first recall the retraction control approach that uses as feedback variable the regularized velocity angle $\gamma^r$ as introduced in [12] and then present a new control approach based on the model (14). In both cases, we consider a hierarchical control scheme, shown in Fig. 3. The inner control loop, the actuation control, is the same for both approaches.

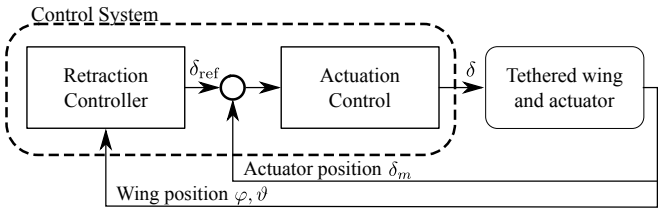


Fig. 3: General hierarchical control structure

The closed loop system for the actuation control loop is given by (see [14] for details)

$$\ddot{\delta}_m = \omega_{\text{cl}}^2\delta_{\text{ref}} - 2\zeta_{\text{cl}}\omega_{\text{cl}}\dot{\delta}_m - \omega_{\text{cl}}^2\delta_m\,, \tag{16}$$

where $\delta_m$ is the actuator's position, $\delta_{\text{ref}}$ is the actuator's position reference, and $\omega_{\text{cl}}$ and $\zeta_{\text{cl}}$ are the natural frequency and damping, respectively, of the actuation control loop. The

actuator's position is linked to the steering deviation $\delta$ by the equation $\delta = K_\delta \delta_m$, where $K_\delta$ is a known constant depending on the mechanical setup of the system. In our case, $K_\delta = 1$.

### A. Velocity Angle Based Controller

The approach presented in [12], which is shortly recalled here, is based on the traction controller developed in [14] using the regularization presented in section II-B.

The retraction controller consists of two nested control loops, compare Fig. 3 and Fig. 4.

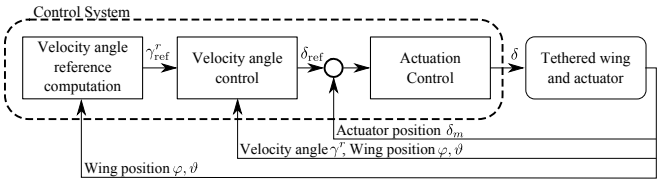


Fig. 4: Control scheme overview using the regularized velocity angle

The inner control loop consists of a proportional controller given by

$$\delta_{\text{ref}} = K_c \left(\gamma^r_{\text{ref}} - \gamma^r\right), \tag{17}$$

where the gain $K_c$ is chosen by the designer. On the basis of the model (12) (where the regularized velocity angle is considered instead of its initial definition (5)), it can be shown that the controller (17) is able to track the desired reference velocity angle. Then, the outer control loop has the task to compute a suitable reference for the inner loop, such that the wing position converges to the border of the wind window, e.g. $\varphi - \varphi_W = \pm\pi/2$, at a given elevation angle $\vartheta_{\text{ref}}$. As seen in the previous section from (12), we have $\gamma^r = \pi/2$ for a static position of the wing with $\varphi - \varphi_W = \pi/2$. This corresponds to a wing position on the left of the wind window as seen from the GU. Similarly, positions on the right can also be considered by changing the sign of the reference.

Using the point-mass model of the tethered wing, it can be shown that there exist equilibrium points at the border of the wind window, whose value are a function (for a given wing) of the steering input $\delta$ and the absolute wind speed. These equilibrium points can be found as usual by setting all time derivatives of the model states to zero and solving (4) for a given steering input. Additionally, they can also be found by numerical simulations of the point-mass model employing a constant steering input. This suggest that these equilibrium points are indeed stable and have a non-empty region of attraction, as it is revealed also by commonly used analysis techniques (see e.g. [17]).

Inspired by the above considerations, the following feedback control strategy has been proposed in [12]:

$$\gamma^r_{\text{ref}} = K_\vartheta(\vartheta_{\text{ref}} - \vartheta) + \frac{\pi}{2}, \qquad K_\vartheta < 0\,. \tag{18}$$

From (18) one can note that if the elevation of the wing is smaller than the reference elevation, then the velocity angle reference is smaller than $\pi/2$, thus demanding the wing to move towards the zenith of the wind window, and vice-versa.

The scalar gain $K_c$ for the velocity angle controller and the scalar gain $K_\vartheta$ for the velocity angle reference computation are chosen by the designer. By using (18) in the outer loop of the control scheme (see Fig. 4), the resulting control system is linear (time varying) and controller gains $K_\vartheta$ and $K_c$ can be found, such that robust stability is achieved in the face of model uncertainty and different wind conditions (see [12] for details). In [12], it is shown with simulations and experiments (see [18] for a short movie) that indeed a single pair $(K_c, K_\vartheta)$ achieves robust stability of the control system.

### B. Wing Elevation Based Controller

In this section we propose a new approach for the retraction controller exploiting the model (14) to compute the reference steering deviation $\delta_{\text{ref}}$, compare Fig. 3. In this way, the designed controller does not rely anymore on an estimate of the velocity angle.

For this purpose, (14) is first linearized around an equilibrium point. As pointed out in section III-A, such an equilibrium point can be found using the point-mass model (4). The resulting linear system is given by

$$\dot{\mathbf{x}} = \begin{bmatrix} 0 & 1 \\ \frac{g\sin(\vartheta)}{r} & -\frac{2\dot{r}}{r} \end{bmatrix} \mathbf{x} + \begin{bmatrix} 0 \\ -\mathcal{C} \end{bmatrix} u\,, \tag{19}$$

where $\mathbf{x} = [\vartheta, \dot{\vartheta}]^T$ and $u = \delta$.

We assume a state feedback controller $K_{\text{SF}}$ of the form

$$z = -K_{\text{SF}}\,\mathbf{x}, \tag{20}$$

where $z = \delta_{\text{ref}}$ and $K_{\text{SF}} = [k_1^{\text{SF}}\ k_2^{\text{SF}}]$. Our goal is to find a matrix $K_{\text{SF}}$ such that the system is stabilized at the chosen equilibrium point. Using a suitable state feedback control technique, e.g. linear quadratic regulator, such a matrix $K_{\text{SF}}$ can be found. In fact, it can be shown that there exists a matrix $K_{\text{SF}}$ for which the system is robustly stabilized in the presence of uncertain, time-varying parameters. For this we consider the error dynamics in $\vartheta$ plus the actuator dynamics (16). The error in $\vartheta$ and $\dot{\vartheta}$ is given as

$$\Delta\vartheta = \vartheta_{\text{ref}} - \vartheta \tag{21}$$

$$\Delta\dot{\vartheta} = \dot{\vartheta}_{\text{ref}} - \dot{\vartheta}\,, \tag{22}$$

where the reference values correspond to a static angular position, i.e. $\dot{\vartheta}_{\text{ref}} = 0$ and $\vartheta_{\text{ref}} \in (0, \pi/2]$, chosen by the user.

Thus, we can state the closed loop dynamics given by (16), (19)-(22), and $\delta = K_\delta \delta_m$ as

$$\begin{bmatrix} \Delta\dot{\vartheta} \\ \Delta\ddot{\vartheta} \\ \dot{\delta}_m \\ \ddot{\delta}_m \end{bmatrix} = \underbrace{\begin{bmatrix} 0 & 1 & 0 & 0 \\ \frac{g\sin(\vartheta)}{r} & -\frac{2\dot{r}}{r} & -\mathcal{C}K_\delta & 0 \\ 0 & 0 & 0 & 1 \\ -\omega_{\text{cl}}^2 k_1^{SF} & -\omega_{\text{cl}}^2 k_2^{SF} & -\omega_{\text{cl}}^2 & -2\zeta_{\text{cl}}\omega_{\text{cl}} \end{bmatrix}}_{A_{\text{cl}}} \begin{bmatrix} \Delta\vartheta \\ \Delta\dot{\vartheta} \\ \delta_m \\ \dot{\delta}_m \end{bmatrix} + w\,, \tag{23}$$

where the term $w$ accounts for model plant mismatch such as the forces exerted by the lines on the actuator. It has to be noted that the model (14) depends on parameters which are difficult to estimate or time-varying. Therefore, system (23)

has time-varying, uncertain linear dynamics characterized by the matrix $A_{\mathrm{cl}}(\Theta)$, where $\Theta = [r, \dot{r}, C_L, E_{eq}, W_0, |\mathbf{v}|]$. However, upper and lower bounds for all of the involved parameters can easily be derived and quadratic stability techniques can be used to check if the chosen $K_{\mathrm{SF}}$ robustly stabilizes the system (see e.g. [19]).

### C. Discussion

We presented two control approaches for the retraction phase, one based on a regularized version of the velocity angle $\gamma$ in section II-B from [12] and one based on the $\vartheta$ dynamics derived from the first principle model (4) in section II-C. In the latter, we exploit a direct link between the input $\delta$ and the angular acceleration $\ddot{\vartheta}$, while the first approach does not directly consider the $\vartheta$ dynamics and relies on the turning rate $\dot{\gamma}$ instead. For the sake of comparison, also in the first approach one can extract the $\vartheta$ dynamics, in particular by assuming that (see [12] for details)

$$\dot{\vartheta} = \frac{|\mathbf{v}^p|}{r}\left(\frac{\pi}{2} - \gamma^r\right), \tag{24}$$

where $|\mathbf{v^p}|$ is the apparent wind velocity projected onto the tangent plane to the wind window at the wing's location. By taking the time derivative of (24) and combining it with (7), and assuming that the apparent wind velocity $\mathbf{v}$ is constant and again that the wing stays at a constant $\varphi$ position, we obtain:

$$\ddot{\vartheta} = -\frac{\rho A C_L}{2rmd_s}\left(1 + \frac{1}{E_{eq}^2}\right)|\mathbf{v}|^2\delta - \frac{g\cos(\vartheta)\sin(\gamma)}{r}. \tag{25}$$

Comparing this equation with the one derived from the first principle model (14), one can see a few differences. First, the second term in the right-hand side of (25) is independent of the reeling speed. This comes from the fact that the $\vartheta$ dynamics in (24) do not consider the influence of the reeling speed $\dot{r}$. The term related to gravity is the same since we assume a $\gamma \approx \pi/2$ for the retraction. Note that, as one would expect, for both models the influence of the additive terms on the angular acceleration become smaller for longer tether length.

The gain relating the input $\delta$ to $\ddot{\vartheta}$, denoted by $\mathcal{C}$ in (14), does not exactly match to the corresponding gain in (25). This difference comes from how the force component in $\vartheta$ direction, $\mathbf{F}\cdot\mathbf{e}_N$, is calculated. In (14), this component is calculated by considering the apparent wind in the tangent plane at the wing's position, i.e. $W_0\sin(\varphi) + r\cos(\vartheta)\dot{\varphi}$ where $W_0\sin(\varphi)$ is the dominating factor, see the appendix. On the other hand, the corresponding term in (24) is $\mathbf{v}^p$ which corresponds, assuming a static angular position at the border of the wind window, to $\mathbf{v}^p \simeq W_0\sin(\varphi)$. Besides these differences, it has to be noted that the structure of the two models is the same, which explains why the corresponding controllers have similar qualitative behavior, as it will be shown in the next section, but with differences in tracking performance.

## IV. Results

We compared the control approach for the retraction phase proposed here with the existing approach from [12] in simulation, employing the non-linear point-mass model for tethered wings (4). The main system's parameters and controller's parameters are shown in Table I and Table II, respectively. The terms relating to $\gamma^r$ apply only to the approach from section III-A and for the state feedback approach an LQ regulator with unitary penalty was used.

In Fig. 5, the trajectories of the wing from launch until the end of the first power cycle are shown. At first, the wing is flown in crosswind conditions, flying figure-eight paths until it reaches the maximum tether length of 150 m, using the controller described in [14]. Then, the retraction phase is started using either the controller based on the regularized velocity angle (17)-(18) or the feedback controller (20), while the tether is reeled-in until a length of 50 m is reached. At that point, the traction phase controller of [14] is used again to complete the power cycle. In Fig. 6, the corresponding time courses of the position angles $\varphi$ and $\vartheta$ during the power cycle are shown. Around 68 s, the controller switches from traction to retraction and tracks the reference $\vartheta_{\mathrm{ref}} = 1$. Note that $\varphi$ becomes larger than $\pi/2$ due to the reel-in speed, indicating that the wing surpasses the GU location against the wind, compare Fig. 5 . Around 140 s, the controller switches from retraction to traction and the wing starts again flying figure-eight paths in crosswind conditions.

Both control approaches lead to very similar results, as it can be seen from Fig. 5-6. The main noticeable difference is the tracking of the $\vartheta$ reference during retraction which is better performed by the approach using a state feedback controller. This is expected, since the latter controller employs directly the elevation angle and its rate, which are both measured with good accuracy, as feedback variables, while the former controller uses the elevation angle to compute a reference for the regularized velocity angle, whose estimate can be inaccurate due to the uncertainty in the wind speed estimation (i.e. the tuning parameter $c$ in (12)). Such uncertainty gives rise to a bias in the feedback variable, which in turn reflects into a larger tracking error. This is shown in Fig. 7 and Fig. 8 where the average tracking error of one retraction phase for different reel-in speeds and different wind speed, respectively. are plotted.

Real-world experiments have already been carried out for the approach using the regularized velocity angle, see [12]. A movie of autonomous power cycles with this approach is available online: [18]. Experiments employing the approach proposed here are planned in the near future.

## V. Conclusion

We developed a new model for the dynamics of the elevation angle of a tethered wing, which we used to design a state feedback controller for the retraction phase of an AWE system with ground-based generation, where the tether is recoiled onto the drums. This approach was compared to a previously developed retraction controller. The new approach was shown to perform better in numerical simulations and we

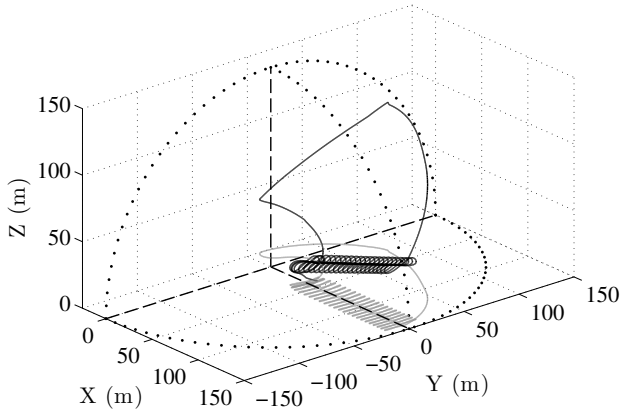


(a) Using the regularized velocity angle for the retraction.

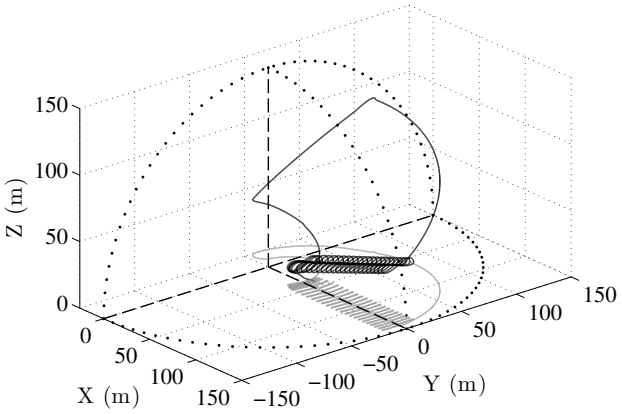


(b) Using a state feedback controller for the retraction.

Fig. 5: 3D trajectory (black) and its projection (gray) on the ground of the tethered wing during one flown power cycle with a reel-in speed of 2.5 m/s and $W_0 = 5$ m/s.

TABLE I: System Parameters

| Name | Symbol | Value | Unit |
|---|---|---|---|
| Wing effective area | $A$ | 9 | $m^2$ |
| Kite span | $d_s$ | 2.7 | m |
| Kite mass | $m$ | 2.45 | kg |
| Tether length | $r$ | [50…150] | m |
| Tether diameter | $d_t$ | 0.003 | m |
| Tether density | $\rho_t$ | 970 | kg/m$^3$ |
| Air density | $\rho$ | 1.2 | kg/m$^3$ |

TABLE II: Control Parameters

| Name | Symbol | Value | Unit |
|---|---|---|---|
| Actuator control loop damping | $\zeta_{\text{cl}}$ | 0.7 | – |
| Actuator control loop natural frequency | $\omega_{\text{cl}}$ | 78 | rad/s |
| Mechanical actuation ratio | $K_\delta$ | 1 | – |
| $\gamma^r$ feedback gain (traction) | $K_{\text{c}}$ | 0.056 | m/rad |
| $\gamma^r$ feedback gain (retraction) | $K_{\text{c}}$ | 0.28 | m/rad |
| $\gamma^r_{\text{ref}}$ feedback gain (retraction) | $K_\vartheta$ | −2.5 | – |
| State feedback control gain 1 (retraction) | $k_1^{\text{SF}}$ | −1.4 | m/rad |
| State feedback control gain 2 (retraction) | $k_2^{\text{SF}}$ | −4.6 | m s/rad |
| Elevation reference (retraction) | $\vartheta_{\text{ref}}$ | 1 | rad |

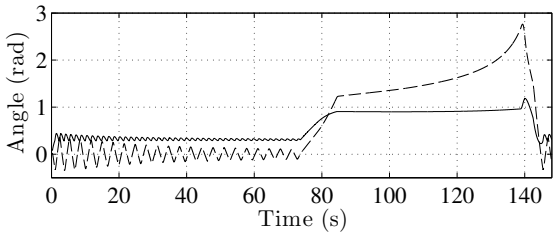


(a) Using the regularized velocity angle for the retraction.

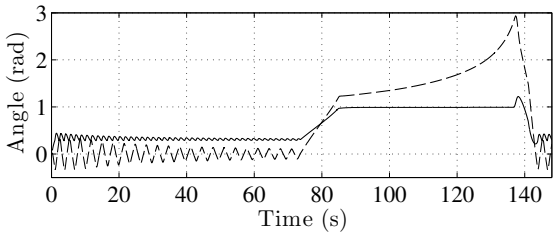


(b) Using a state feedback controller for the retraction.

Fig. 6: Time courses of $\varphi$ (dashed) and $\vartheta$ (solid) of one power cycle with a reel-in speed of 2.5 m/s and $W_0 = 5$ m/s.

expect it to outperform the previous strategy in experiments since it does not need an estimate of the velocity angle and directly relies on angular measurements. Together with the traction controller in [14] the approach presented here can be used to achieve fully autonomous power cycles. The controller is based on a hierarchical structure and is able to stabilize the wing's trajectory at a position at the border of the wind window, where the traction force is minimal. Few parameters, that can be easily tuned, are involved in the design. The approach employs the steering deviation as control input and it can stabilize the wing's elevation robustly against different tether lengths and reeling speeds. Hence, the latter can still be optimized to maximize the energy output of the system.

## Appendix
## Elevation Dynamics

*Proof of Proposition 1.* For the sake of simplicity of notation we drop the dependence of time-varying variables from $t$. We start with the expression given in [14] for the force $\mathbf{F}$ in $\mathbf{e}_N$ direction:

$$\begin{aligned}\mathbf{F}\cdot\mathbf{e}_N = F_L\,(&\cos(\eta)\sin(\Delta\alpha)\cos(\xi)-\\ &(\sin(\eta)\sin(\Delta\alpha)+\cos(\Delta\alpha)\psi)\sin(\xi))-\\ &F_{D,eq}\cos(\Delta\alpha)\cos(\xi)-mg\cos(\vartheta)\,,\end{aligned}\tag{26}$$

where $\xi$ is the heading of the wing, $\Delta\alpha$ the angle between the apparent wind and the tangent plane $(\mathbf{e}_N, \mathbf{e}_E)$, and $\psi$ the roll angle of the wing. The mass of the wing plus the added mass of the tether is denoted by $m$ and $g$ is the gravity. The angle $\eta$ is defined as (see e.g. [20])

$$\eta = \arcsin(\tan(\Delta\alpha)\tan(\psi))\,.\tag{27}$$

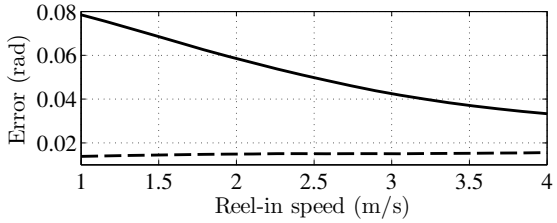


Fig. 7: Average $\vartheta$ tracking error for different reel-in speeds for the regularized velocity angle based control (solid) and for the state feedback control (dashed) during one retraction phase with $W_0 = 5\,\mathrm{m/s}$.

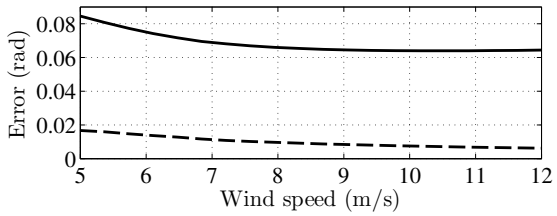


Fig. 8: Average $\vartheta$ tracking error for different wind speeds $W_0$ using the regularized velocity angle based control (solid) and the state feedback control (dashed) during one retraction phase with a reel-in speed of 2.5 m/s.

$F_L$ is the lift force and $F_{D,eq}$ the equivalent drag force including also the tether drag:

$$F_L = \frac{1}{2}\rho A C_L |\mathbf{v}|^2 \tag{28}$$

$$F_{D,eq} = \frac{1}{2}\rho A C_{D,eq} |\mathbf{v}|^2 , \tag{29}$$

where $\rho$ is the air density, $A$ is the effective area of the wing, $C_L$ and $C_{D,eq}$ are the lift coefficient and equivalent drag coefficient (for details see e.g. [14]), and $\mathbf{v}$ is the apparent wind velocity.

By Assumption 1-2 and considering the equilibrium of the lift and drag force in the direction of the wing's heading $\xi$, projected on the tangent plane to the sphere at the wing's location, we have (see [21]):

$$\frac{\sin(\Delta\alpha)}{\cos(\Delta\alpha)} = \frac{1}{E_{eq}} \doteq \frac{C_{D,eq}}{C_L} , \tag{30}$$

where $E_{eq}$ is the equivalent efficiency of the wing. By (30) we can see that $\Delta\alpha$ is small for a reasonable wing efficiency of $4-6$.

By Assumption 3 and (30) we see that (27) simplifies to

$$\eta = \frac{1}{E_{eq}}\psi = \frac{1}{E_{eq} d_s}\delta , \tag{31}$$

where $d_s$ is the span of the wing.

The heading of the wing $\xi$ is given by the apparent wind vector $\mathbf{v}$ defined with (3), (9), and

$${}_L\mathbf{v}_W = \begin{pmatrix} -W_0 \sin\vartheta \cos(\varphi) \\ -W_0 \sin(\varphi) \\ -W_0 \cos\vartheta \cos(\varphi) \end{pmatrix} . \tag{32}$$

where $W_0$ is the nominal wind speed and it is assumed that the wind vector is horizontal and in $\mathbf{e}_x$ direction. Therefore, the heading of the wing can be written as:

$$\xi = \arctan\left(\frac{-\mathbf{v}\cdot\mathbf{e}_E}{-\mathbf{v}\cdot\mathbf{e}_N}\right) = \arctan\left(\frac{W_0 \sin(\varphi) + r\cos(\vartheta)\dot{\varphi}}{W_0 \sin(\vartheta)\cos(\varphi) + r\dot{\vartheta}}\right) \tag{33}$$

By using (26) together with (28)-(31) and (33) we obtain:

$$\mathbf{F}\cdot\mathbf{e}_N = \frac{\rho A C_L}{2 d_s}\left(1 + \frac{1}{E_{eq}^2}\right)(W_0 \sin(\varphi) + r\cos(\vartheta)\dot{\varphi})|\mathbf{v}|\delta - mg\cos(\vartheta) . \tag{34}$$

Equation (13), by Assumption 2, can now be rewritten as

$$\ddot{\vartheta} = -\mathcal{C}\delta - \frac{g\cos(\vartheta) + 2\dot{\vartheta}\dot{r}}{r} , \tag{35}$$

where

$$\mathcal{C} = \frac{\rho A C_L}{2 r m d_s}\left(1 + \frac{1}{E_{eq}^2}\right) W_0 \sin(\varphi)|\mathbf{v}| . \tag{36}$$

## REFERENCES


[1] L. Fagiano and M. Milanese, "Airborne wind energy: an overview," in *American Control Conference 2012*, Montreal, Canada, 2012, pp. 3132–3143.

[2] M. Diehl, R. Schmehl, and U. Ahrens, Eds., *Airborne Wind Energy*, ser. Green Energy and Technology. Springer Berlin Heidelberg, 2014.

[3] M. L. Loyd, "Crosswind kite power," *Journal of Energy*, vol. 4, no. 3, pp. 106–111, June 1980.

[4] M. Canale, L. Fagiano, and M. Milanese, "High altitude wind energy generation using controlled power kites," *IEEE Transactions on Control Systems Technology*, vol. 18, no. 2, pp. 279 –293, Mar. 2010.

[5] A. Ilzhöfer, B. Houska, and M. Diehl, "Nonlinear MPC of kites under varying wind conditions for a new class of large-scale wind power generators," *International Journal of Robust and Nonlinear Control*, vol. 17, pp. 1590–1599, 2007.

[6] J. H. Baayen and W. J. Ockels, "Tracking control with adaption of kites," *IET Control Theory and Applications*, vol. 6, no. 2, pp. 182–191, 2012.

[7] P. Williams, B. Lansdorp, and W. Ockels, "Optimal crosswind towing and power generation with tethered kites," *Journal of guidance, control, and dynamics*, vol. 31, no. 1, pp. 81–93, 2008.

[8] B. Houska and M. Diehl, "Optimal control for power generating kites," in *European Control Conference (ECC), Kos, Greece, 2.-5. July*, 2007.

[9] S. Costello, G. Franois, and D. Bonvin, "Real-time optimization for kites," in *Proceedings of the IFAC Workshop on Periodic Control Systems, Caen, France, 3.-5. July*, 2013, pp. 64–69.

[10] M. Diehl, "Real-time optimization for large scale processes," Ph.D. dissertation, Ruprecht-Karls-Universität Heidelberg, June 2001.

[11] C. Jehle and R. Schmehl, "Applied tracking control for kite power systems," *Journal of Guidance, Control, and Dynamics*, 2014.

[12] A. Zgraggen, L. Fagiano, and M. Morari, "Retraction phase control using regularized velocity angle," ETH Zurich, Tech. Rep., October 2013, technical report #TR_ZFM_151013. Available: http://control.ee.ethz.ch/~aldoz/docs/TechRep/ZFM_TR_151013.pdf.

[13] Swiss Kite Power, "Windisch, Switzerland [Online]," Sep. 2013, available: http://www.swisskitepower.ch/.

[14] L. Fagiano, A. U. Zgraggen, M. Morari, and M. Khammash, "Automatic crosswind flight of tethered wings for airborne wind energy: modeling, control design and experimental results," *IEEE Transactions on Control Systems Technology*, 2013, in press, online version available.

[15] M. Erhard and H. Strauch, "Control of towing kites for seagoing vessels," *Control Systems Technology, IEEE Transactions on*, vol. 21, no. 5, pp. 1629–1640, 2013.

[16] A. Zgraggen, L. Fagiano, and M. Morari, "On real-time optimization of airborne wind energy generators," in *Conference on Decision and Control*, Florence, Italy, 10-13 Dec 2013, pp. 385–390.

[17] H. K. Khalil, *Nonlinear Systems*, 3rd ed. Prentice Hall, 2001.

[18] Swiss Kite Power, "Experimental test movie ," Oct. 2013, available on–line: http://youtu.be/yDRc3Ze4GAM.

[19] F. Amato, *Robust Control of Linear Systems Subject to Uncertain Time-Varying Parameters*, ser. Lecture Notes in Control and Information Sciences. Springer Berlin Heidelberg, 2006, vol. 325.

[20] I. Argatov, P. Rautakorpi, and R. Silvennoinen, "Estimation of the mechanical energy output of the kite wind generator," *Renewable Energy*, vol. 34, no. 6, pp. 1525 – 1532, 2009.

[21] L. Fagiano, M. Milanese, and D. Piga, "Optimization of airborne wind energy generators," *International Journal of Robust and Nonlinear Control*, vol. 22, no. 18, pp. 2055–2083, 2012.